metabolites

MDPI

Article

Exploring UVA1-Induced Metabolic Effects in Different In Vitro, Ex Vivo, and In Vivo Systems

Irina Ivanova [1,*], Teodora Svilenska [1], Tim Maisch [1], Wolfram Gronwald [2], Dennis Niebel [1], Martin Lehmann [3], Andreas Eigenberger [4], Lukas Prantl [4], Mark Berneburg [1], York Kamenisch [1,†] and Bernadett Kurz [1,*,†]

[1] Department of Dermatology, University Hospital Regensburg, 93053 Regensburg, Germany
[2] Institute of Functional Genomics, University of Regensburg, Am BioPark 9, 93053 Regensburg, Germany
[3] Mass Spectrometry of Biomolecules (MSBioLMU), LMU München, Großhaderner Straße 2-4, 82152 Planegg-Martinsried, Germany
[4] Department for Plastic, Hand & Reconstructive Surgery, University Hospital Regensburg, 93053 Regensburg, Germany
* Correspondence: irina.ivanova@ukr.de (I.I.); bernadett.kurz@ukr.de (B.K.)
† These authors contributed equally to this work.

Abstract

Background/Objectives: Studying the role of UV-induced metabolic changes in skin physiology, and especially skin diseases, has gained importance in both medicine and cosmetics. With the development of new technologies, a variety of approaches have been implemented to model these metabolic effects. In this study, we explore the reproducibility of the UVA1-induced metabolic changes observed in different in vitro, ex vivo, and in vivo systems with escalating complexity. Our aim is to elaborate on the role of experimental setups in the reliable representation of in vivo data in other systems. **Methods:** Metabolic profiles post UVA1 treatment were assessed in skin cell culture, skin explants, and intact skin. For cell culture and explants, the metabolites from the culture medium were assessed via 1D-CPMG NMR. Intact skin samples were collected via microdialysis and the resulting dialysate was measured with GC–TOF-MS. **Results:** Data show that, despite great metabolic variations between the systems, several metabolites, such as glutamic acid, succinic acid, and threonine, change in a similar manner across multiple systems after UVA1 irradiation, including in vivo settings. Some metabolites, like phenylalanine, citric acid, and pyruvic acid, show similar UVA-mediated metabolic patterns between corresponding in vitro and ex vivo systems, but do not overlap well with in vivo data. **Conclusions:** Our findings emphasize the need for a metabolite-by-metabolite approach when deciding on the proper experimental system to perform UV irradiation experiments with regard to cutaneous physiology.

Keywords: UVA; human skin metabolism; microdialysis; NMR; GC–TOF-MS

Academic Editor: Michele Costanzo

Received: 12 December 2025
Revised: 21 January 2026
Accepted: 26 January 2026
Published: 29 January 2026

1. Introduction

The skin is the largest organ of the human body and its barrier to the outside world. As such, it is subject to a variety of chemical and physiological stressors, among which is ultraviolet (UV) radiation [1,2]. Based on wavelength, UV radiation can be subdivided into three major types that are relevant for human health—UVC (100–280 nm), UVB (280–315 nm), and UVA (315–400 nm) [3,4]. From the solar spectrum reaching the Earth's surface, UVA (consisting of UVA2 (315–340 nm) and UVA1 (340–400 nm)) is the predominant component, constituting 95% of the overall dose as opposed to UVB [4]. Exposure to UV radiation can lead to a variety of macroscopic and microscopic changes, including wrinkle formation

(photoaging), barrier function disruption, cell death, inflammation, DNA damage, and cancer. Through a combination of direct energy transfer and indirect radical formation, UV radiation can cause DNA modifications, lipid peroxidation, and protein misfolding. It can also result in changes in the metabolism of the skin.

Due to the aggressive nature but short half-life of UV-induced reactive species such as peroxyl, hydroxyl, and superoxide radicals upon irradiation, the metabolic response in the form of radical quenchers (for example, pyruvic and lactic acids and glutathione) forms the first line of defense of the skin [1,5]. Compared to proteomic and genomic studies, assessing the metabolic profile after irradiation gives a unique insight into the immediate, real-time physiological changes in the effected tissue. Aberrations in the skin metabolism can lead to inflammation, disturbance in the commensal flora of the skin, immune evasion by tumors, and premature cell death. Thus, the study of skin metabolism is pivotal in all fields of dermatology—cancer research [6,7], inflammatory skin diseases [8,9], aging [10,11], skin homeostasis, and wound healing [12,13]. Therefore, understanding the short- and long-term effects of UV radiation on skin metabolism can provide further insight not only into the etiology of photoaging and photosensitive skin diseases like lupus erythematosus and polymorphic light eruption, but also aid skin cancer research by supporting the development of new sun protective strategies and treatments.

There are many established techniques to collect and evaluate the metabolic profile of intact skin [14], but implementing them in patient studies has its drawbacks [15]. Although performing a skin biopsy is the easiest way to acquire material for metabolic testing, it provides only a momentary "snapshot" of the skin's condition. It is not suitable for longitudinal studies due to the increased burden on the patient resulting from multiple sample collections. Thus, the implementation of minimally invasive techniques for skin sample collection, such as microdialysis, is gaining popularity as a means of in vivo sample collection [15,16]. In addition to its minimal invasiveness, microdialysis also allows for repeated sampling from a single spot, making it possible to perform in vivo time kinetics with a singular catheter insertion. It also abolishes the need for complex tissue preparation and homogenization that are required for biopsy samples, allowing for quick and reliable sample collection in small time increments.

Still, implementing cost-effective, scalable, and homogeneous in vitro and ex vivo systems is an appealing alternative to in vivo testing. Each of these systems, however, has its advantages and disadvantages that need to be considered when choosing an experimental setup [15,17–21].

Some advantages of in vitro systems are condition reproducibility, availability, and speed, combined with low ethical considerations [21]. A large drawback is the over simplistic depiction of otherwise complex physiological processes by implementing monocultures or simple co-cultures [22,23]. Under these conditions, metabolites derived from the subcutaneous fatty layer (for example, fatty acids, glycerol, and valine) and their influence on dermal and epidermal cells cannot be assessed. Interactions between cells, metabolites, and the extracellular matrix (ECM) are also difficult to assay, although there are ECM substitutes in development [24]. Furthermore, artificial culturing media can influence cellular behavior and experimental readout [25,26]. Classical Dulbecco's modified Eagle's medium and Minimum Essential Medium Alpha, for example, are typically formulated with pyruvate concentrations ten times higher than the ones found in human blood [27]. Considering the antioxidative properties of pyruvate, its concentration in the medium can greatly influence the outcome of experiments that deal with oxidative stressors such as diverse chemical compounds or UV irradiation [1,25,28]. Another drawback is the fact that many cells, used in in vitro cultures, are immortalized, rendering abnormal physiology [19].

Compared to natural skin, full-thickness skin models also have the caveat that, depending on the ECM substitute used for the tissue generation, the skin equivalent can acquire variable properties, which should be considered during experiment planning [29]. Still, skin equivalents can be used to model cell–cell and cell–ECM interactions, which are crucial when studying metabolic events. As a drawback, 3D scaffolding and organotypic cultures still lack the morphological and cellular complexity of ex vivo and in vivo systems [30,31]. Especially challenging is replicating the immunological component of the skin. Mimicking immunological reactions is crucial for studying UV-induced inflammation and the resulting metabolic regulations—two components indispensable when conducting research on UV-induced autoimmune diseases [32,33]. Differences in the lipid composition between native skin and skin reconstructs also present an issue, especially when exploring the effects UV radiation has on skin permeability and fatty acid metabolism [34]. Another issue present during the UV irradiation of skin equivalents is their thickness. Some artificially grown constructs, although presenting all functional layers, are much thinner than natural skin. Considering the different penetration capabilities of the various UV wavelengths [35], thinner constructs can lead to inaccurate results when studying penetration-dependent metabolic gradients. In addition, skin equivalents require specialized culturing conditions and knowledge to produce, leading to increased costs and personnel requirements [36,37]. Nevertheless, full-thickness skin equivalents represent a good balance of reproducibility and complexity compared to cell monolayers.

Ex vivo cultures, namely skin explants, breach the gap between in vitro and in vivo systems, but significant differences remain when compared to an intact living organism [38]. On the plus side, skin explants possess resident immune cells, which allow for better assessment of immune-dependent metabolic changes like the release of prostaglandins after UV irradiation [32]. However, just like in vitro systems, ex vivo explants rely on artificial media for nutrient supplementation, which can impact and falsify the collected data [39,40]. Furthermore, these cultures lack an interaction with surrounding organs and bodily fluids that can potentially influence the experimental outcome and the data interpretation [23]. This results in a knowledge gap when it comes to the effects of liver- or kidney-derived metabolites (for example, creatine) on the UV response.

Performing experiments on living organisms can yield the most complete data during the experimental proceedings, but it comes with many ethical considerations [23]. Expenses, difficult recruitment of probands, system complexity, specialized personnel requirements, as well as the invasiveness of experimental procedures are only a few of the criteria that need to be taken into consideration [21,41]. Furthermore, it is difficult to manipulate the environmental variables, and there is a greater variation between test subjects, requiring large experimental cohorts [23]. An additional concern when performing metabolic studies, even with minimally invasive techniques like microdialysis, is the influence of anesthesia on the metabolic profile [42]. There have been studies showing strong influences on the skin oxidative metabolism by different anesthetic compounds [43,44]. Furthermore, the implantation of a microdialysis catheter can lead to inflammation that could mask weaker UV-induced immune responses.

Another point of concern in using animal models is the translation of the observed results to human conditions. Despite being useful models for toxicological and immunological studies, mice and pigs (the two most common organisms used in dermatological research) still exhibit different metabolic rates compared to humans. This can lead to differences in reactive oxygen species (ROS) production and quenching [45,46], which can subsequently result in data anomalies when exploring UV-induced oxidative damage and antioxidant metabolism. Such experimental uncertainties can have a negative influence on studies concerning photoaging, photo carcinogenesis, and photoprotection. Furthermore, in the case of mouse skin, a major problem for conducting UV experiments is the hair

follicle density. Humans have an overall lower hair follicle density than mice [47–50]. It has been shown that hair follicles can act as fiber optic units and transduce UV radiation into the skin, thus influencing the cell reaction and metabolic profile after irradiation [51]. Although using hairless mice might seem like a logical solution to the problem, some strains exhibit dermal cysts, sebaceous gland hyperplasia, and rudimentary hair follicles that change the structural and chemical composition of the skin [52]. Furthermore, animal models have less skin vascularization than humans [50], influencing the speed at which nutrients and antioxidants are replenished in the skin after UV exposure.

With this work, we want to emphasize the importance of choosing and combining experimental setups when performing metabolic studies, especially when external stressors such as UV radiation are co-assessed. Due to the diverse strengths and weaknesses of the experimental systems listed above, the current study focuses on elaborating on the data reproducibility and transferability between in vitro, ex vivo, and in vivo models in the context of UVA1-induced metabolic changes. We, therefore, irradiated primary human fibroblasts, immortalized keratinocytes, and skin explants. We then compared their metabolic profiles to the metabolic profile obtained from in vivo UVA1-treated skin through microdialysis. Metabolites were analyzed by high-resolution ^{1}H NMR spectroscopy and hyphenated mass spectrometry.

2. Materials and Methods

Determining UVA1 irradiation dose for microdialysis probands

We irradiated the lower back of three healthy volunteers (2 female, 1 male; the test subjects differed from the skin flap donors used for the ex vivo culture) with increasing doses of UVA1 to determine the skin-specific minimal erythema dose (MED) (Supplemental Figure S2a,d). The irradiation for the microdialysis experiment was subsequently performed on the outer forearm arm of the probands with an adjusted irradiation dose of 1.5-fold MED, resulting in a dose range of 28–40 J/cm^2. This increased irradiation dose is justified by the weaker reaction of typically sun-exposed areas, such as the outer side of the forearms, in comparison to sun-protected areas like the lower back [53].

Microdialysis and irradiation of probands

Cutaneous microdialysis is a cutting-edge, minimally invasive technique that allows the collection of data from cutaneous interstitial fluid in real time (Supplemental Figure S2b). In this study, we assayed the UVA1-induced metabolic changes in three healthy probands—2 female and 1 male, aged between 24 and 53.

Briefly summarized, the procedure was performed as follows. A 5 × 5 cm^2 area on the extensor side of the subjects' lower arm was disinfected and treated with a topical anesthestetic (Lidocaine/Prilocaine cream), EMLA® (Aspen GmbH, Munich, Germany) for 1 h. The cream was then removed. A 21G cannula introducer was inserted through the skin between the epidermis and the dermis (0.6–0.8 mm depth), resulting in an entrance and an exit puncture. A 66 Linear Microdialysis Catheter (M Dialysis AB, Stockholm, Sweden) with a 30 mm semi-permeable membrane (0.5 mm diameter, cut-off 100 kDa) was inserted into the distal end of the introducer. The cannula was then removed, positioning the catheter membrane in the tissue. The microdialysis catheter was flushed with perfusion solution (physiological saline solution 0.9% NaCl, Fresenius Kabi, Bad Homburg; Germany) for 5 min at a rate of 5 µL/min, and afterwards, a flush sequence of 30 min at a rate of 2 µL/min was initiated to equilibrate the semi-permeable membrane.

After the equilibration, the sample collection for time point T: 0-0 (time before irradiation, later referred to as "Control") was initiated (flow rate 2 µL/min). A total of 1.5 h after the catheter flow-through collection began, the microdialysis was paused and the acquired

sample was immediately frozen at −20 °C. Subsequently, the area of the inserted catheter of each proband was irradiated with the individual 1.5 MED. During the irradiation, the sample collection for time point T: A-0 (time during and immediately after irradiation, later referred to as "UVA") was initiated (flow rate 2 µL/min). Collection time and sample storage were identical to the procedure described for T: 0-0. Samples were transferred to −80 °C for long-term storage and subsequent analyses (for graphical representation, see Supplemental Figure S2e).

The microdialysis catheter was subsequently removed from the skin.

Counting the removal of anesthesia, preparation and catheter insertion, and washing sequence, the time elapsed between the removal of anesthesia and the first sample collection amounted to >55 min. The time between catheter insertion and the first sample collection amounted to >40 min. This recovery time before the initiation of the experiment is consistent with the already published literature on the topic [54–58].

Cell culture

Primary Human Fibroblasts (Re5)

To obtain primary human fibroblasts, a skin biopsy sample was taken from the tissue of a healthy donor. The whole skin biopsy was placed on a Primaria cell culture dish (#353801, Corning, Kaiserslautern, Germany), containing a single drop of DMEM-Cipro medium (DMEM medium (P04-01548, PAN Biotech, Aidenbach, Germany), 10% FCS (AC-SM-0161, Anprotec, Bruckberg, Germany), 1 g/L (5.5 mM) glucose (G8644, Sigma-Aldrich/Merck, Germany), 1 mM pyruvate (#11360070, Thermo Fisher Scientific, Waltham, MA, USA), 2 mM L-glutamine (G7513, Sigma-Aldrich/Merck Taufkirchen, Germany), and 1% Ciprofloxacin (200 mg/100 mL infusion solution, 64,689.00.00, Fresenius Kabi, Bad Homburg, Germany). It was incubated for 30 min at 37 °C to ensure adhesion of the skin sample on the dish surface. Afterwards, 3 mL DMEM-Cipro was added to the skin sample. It was cultivated at 37 °C, 5% CO_2, until fibroblast-outgrowth was sufficient for a transfer to a T25 cell culture flask, where obtained cells were cultured in DMEM without Ciprofloxacin, and used for further experiments. The isolated primary fibroblasts were designated as Re5.

Immortalized Keratinocytes (HaCaT)

Human immortalized keratinocytes (HaCaT) were purchased from Cell Lines Service (Eppelheim, Germany) and cultured in standard DMEM medium without Ciprofloxacin at 37 °C, 5% CO_2.

Skin explant culture ex vivo

Un-irradiated human abdominal flap skin from three healthy donors was acquired from the Department of Plastic Surgery of the University of Regensburg, Germany. The abdominal flaps were collected during planned abdominoplasties and would otherwise have been discarded.

Prior to the beginning of the experiments, the subcutaneous fat was removed from the skin section. The samples were divided into eight punches of 8 mm diameter—two for un-irradiated control with pyruvate, two for un-irradiated control without pyruvate, two for irradiated control with pyruvate, and two for irradiated control without pyruvate. Each of the 8 mm punches was placed on a piece of sterile gauze in order to facilitate floatation, thus providing a liquid–gas interface culture condition. The punches were then transferred to a 12-well plate with 2 mL DMEM (1 mM/0 mM pyruvate). Sterile gauze without skin samples was placed in control wells containing 2 mL DMEM (1 mM/0 mM pyruvate). Irradiation commenced immediately after establishment of the floatation culture. During the irradiation experiment, the plates with floatation cultures were kept at 37 °C, 5% CO_2.

Irradiation protocol and sample collection in vitro and ex vivo

The irradiation of skin cells and skin explants was performed with a Sellamed-Lamp (Sellas Medizinische Geräte GmbH, Ennepetal, Germany) with emission spectrum 340–420 nm (see Supplemental Figure S1a).

Skin explants

Immediately after preparing the Ø 8 mm floatation culture from the donor skin, culture plates were irradiated with 6 J/cm^2 UVA1 (see Supplemental Figure S1c). Wells containing medium and floatation gauze without skin tissue were irradiated as controls. After the irradiation, the explants were given 4 h of rest (in a 5% CO_2 incubator, at 37 °C) before the treatment was repeated. In total, 3 UVA1 treatments were performed per day over the span of 2 days. At day 3, a single UVA1 irradiation was performed and after 4 h of rest, the culture medium was collected for metabolic studies. The cumulative irradiation dose for the duration of the experiment was 42 J/cm^2, lying in the upper dose range applied in vivo. This was to assure that a robust metabolic response could be detected. The experimental duration was set to 2.5 days to take the limited viability of explant cultures into account [59].

Skin cells

One day before irradiation, the cells were seeded at a density of 5×10^4 cells per well on a 6-well plate in DMEM with 1 mM/0 mM pyruvate and incubated overnight.

At the beginning of irradiation, the medium was aspirated from each well. Cells were irradiated in 1 mL PBS. For graphical representation of the irradiation protocol see Supplemental Figure S1b. The dose of UVA1 per single irradiation was set at 6 J/cm^2. Following irradiation, the PBS was aspirated and 5 mL fresh medium with 1 mM/0 mM pyruvate was added to the corresponding wells after the first irradiation. Before all subsequent irradiations, the medium was aspired and collected in separate falcons and returned to the corresponding wells afterwards.

A total of 3 irradiations was performed per day with a 4 h resting period between each irradiation and an overnight rest after the final daily irradiation. The whole treatment lasted for four days.

The time for sample collection is crucial for system comparability. For the cell monolayers and skin explants, we took into consideration previously published data on metabolite diffusion through skin [60,61] and set a minimum collection time post-treatment to 4 h. Compared to skin explant culture where the metabolic yield is provided by multiple layers of cells, in cell culture it is the result of a single cell monolayer. To assure metabolite enrichment, we postponed medium collection overnight after irradiation in accordance with our preliminary studies.

Nuclear magnetic resonance (NMR) measurement of skin and cell culture supernatants

After the UVA treatment, the supernatant from the cell samples as well as control media without cells was preserved at −80 °C before further processing. In preparation for the NMR measurements, 400 µL from each sample was mixed with 200 µL of 0.1 M phosphate buffer, pH 7.4, which contained 3.9 mM boric acid to impair the growth of bacteria, and 50 µL of 0.75 (wt) trimethylsilylpropanoic acid (TSP; Sigma-Aldrich, Germany) in deuterium oxide (D_2O) as internal reference standard and subsequently pipetted in glass NMR-vials. Additionally, 10 µL of 81.97 mmol/L formic acid (FA) were added as a second internal reference standard that is not prone to protein binding.

All NMR experiments were performed at 298 K on a 600 MHz Bruker Avance III HD spectrometer (Bruker BioSpin GmbH, Ettlingen, Germany) using a triple resonance (^{1}H, ^{13}C, ^{15}N, ^{2}H lock) cryogenic probe with z-gradients in combination with a Bruker SampleJet sample changer (Bruker BioSpin GmbH, Germany).

Spectra of cell culture supernatants and control media were acquired employing a 1D ^{1}H Carr-Purcell-Meiboom-Gill (CPMG) pulse sequence to achieve effective suppression of macromolecular signals. These broad macromolecular signals will overlap with signals of small molecules if not suppressed and hamper their identification and quantification. Due to their size, macromolecules such as proteins tumble in solution much slower than small molecules. As a result, the T_2 relaxation times, which determine the time span in which an NMR signal may be observed, are much smaller for macromolecules than for small molecules such as typical metabolites. Therefore, employing a T_2 relaxation filter, as incorporated in the CPMG pulse sequence, allows efficient suppression of macromolecular signals, whereas signals of small molecules are only minimally impacted. This leads to clean 1D proton NMR spectra in which metabolite identification and quantification is considerably eased.

The acquired data were semi-automatically Fourier-transformed to 128 k real data points, phase corrected, and baseline optimized with TopSpin 4.0.7 (Bruker BioSpin GmbH, Ettlingen, Germany). Chenomx 8.6 (Chenomx Inc., Edmonton, AB, Canada) was employed for identification and quantification of metabolites from 1D NMR spectra. The concentration of metabolites in the cell supernatants (C_s) and in fresh medium (C_{med}) were used together with the sample volume (vols) used in the 6-well plates used for cell culture—5 mL—and the end number of cells to calculate the amounts of consumed or secreted metabolites per million cells. For that, the following equation was used:

$$\mathbf{mmol} \Big/ \mathbf{10^6\ cells} = \frac{(\mathbf{C_{med}} * \mathbf{AVERAGE\ vol_s[L]}) - (\mathbf{C_s} * \mathbf{vol_s[L]})}{\mathbf{10^6\ cells}} \quad (1)$$

Since the skin explants were all the same diameter and thickness, and the volume culture medium per well was constant, the NMR data did not require further normalization. Only the corresponding blank-medium (C_{med}) values for each treatment were subtracted from the samples (C_s) to visualize the net metabolic change coming from the interaction between UVA irradiation and the skin:

$$\mathbf{mM} = \mathbf{C_{med}} - \mathbf{C_s} \quad (2)$$

GC–TOF-MS measurement of microdialysates

Microdialysate metabolomics analysis was conducted via gas chromatography coupled to time-of-flight mass spectrometry (GC–TOF-MS). Therefore, 80 µL of the dialysate was mixed with 160 µL methanol. Measurements of 80 µL of pure microdialysis perfusion solution mixed with 160 µL methanol were used as a blank sample. All samples were dried using a rotational vacuum concentrator (Alpha RVC, Martin Christ Gefriertrocknungsanlagen GmbH, Osterode am Harz, Germany).

Metabolite analysis was modified from previous publications [62–64]. In general, the dry pellet was resuspended in 100 µL methanol/water (50:50 *v*/*v*). After vortexing, the samples were sonicated for 5 min and centrifuged at maximum speed. A measurement of 60 µL was dried in vacuo and stored at −80 °C. For derivatization, the pellet was resuspended in 10 µL of methoxyaminhydrochloride (20 mg mL^{-1} in pyridine) and incubated for 90 min at 40 °C. After the addition of 20 µL of BSTFA (N,O-Bis[trimethylsilyl]trifluoroacetamide) containing 2.5 µL retention time standard mixture of linear alkanes (n-decane, n-dodecane, n-pentadecane, n-nonadecane, n-docosane, n-octacosane, n-dotriacontane), the mix was incubated at 40 °C for a further 45 min. A measurement of 1 µL of each sample was injected into a GC–TOF-MS system (Pegasus HT, Leco, St. Joseph, MI, USA). Samples were automatically processed by an autosampler system (Combi PAL, CTC Analytics AG, Zwingen, Switzerland). The carrier gas was helium at a constant flow rate of 1 mL/min. Gas

chromatographic separation was performed on an Agilent GC (7890A, Agilent, Santa Clara, CA, USA) using a 30 m VF-5ms column with 10 m EZ-Guard column. The temperature of the split/splitless injector of the transfer line and of the ion source was kept at 250 °C. The initial oven temperature (70 °C) was continuously increased to 350 °C by 9 °C/min. Metabolites were separated and ionized by electron ionization at 70 eV. Mass spectra were recorded at 20 scans s^{-1} with an m/z 50–600 scanning range. Chromatograms and mass spectra were evaluated using ChromaTOF 4.72 and TagFinder 4.1 software [65].

All sample readouts were obtained as "counts" (peak intensity at maximum) and were normalized to volume. The counts for the blank samples were subtracted from all proband samples. To assess changes in the metabolite abundance before and after irradiation, a fold change for each metabolite was calculated according to the following formula:

$$\mathbf{Foldchange_x} = \frac{\mathbf{Count_{UVA}}}{\mathbf{Count_c}} \quad (3)$$

$Count_{UVA}$ stands for the readout of metabolite (x) after UVA irradiation, $Count_c$ stands for the readout of metabolite (x) prior to UVA treatment. A fold change greater than 1 indicated metabolite increase after irradiation. A fold change smaller than 1 indicated metabolite decrease after irradiation.

Cell count and viability measurement

To determine the number of cells, as well as their viability, a LUNA-FL Dual Fluorescence Cell Counter (Logos Biosystems, Aligned Genetics, Inc., Dongan-gu, Anyang-si, Gyeonggi-do, Republic of Korea) in combination with Acridine orange/Propidium iodide (AO/PI) staining was used. To perform the actual cell count, 18 µL of cell suspension were mixed with 2 µL AO/PI dye (F23001-LG, BioCat, Heidelberg, Germany). From this mixture, 10 µL were pipetted on a LUNA cell counting slide and measured in fluorescence modus with LUNA-FL.

Nitroblue tetrazolium chloride (NBTC) staining

NBTC is a redox indicator. It is reduced by cell-bound NADH-diaphorase, which has activity only in viable cells. This leads to the production of a blue granular precipitate in living cells that can be distinguished microscopically from unstained dead cells. The NBTC staining of mouse skin explant was performed as follows.

After irradiation, human skin punches were shock-frozen in liquid nitrogen. The samples were then embedded in tissue-tek and cut to 8 µm thick slices via cryotome. To perform the vitality staining, a master mix containing 1 mL NADH (N6879, Sigma-Aldrich/Merck, Taufkirchen, Germany), 2.5 mL NBTC (N6876, Sigma-Aldrich/Merck, Taufkirchen, Germany), 1 mL PBS (pH 7.4), and 0.5 mL ringer solution (9517170, B.Braun AG, Melsungen, Germany) was added. From the master mix, 60 µL was pipetted on each section and the sections were incubated for 15 min at room temperature. Afterward, the reaction was stopped in PBS and the samples were covered using Aquatex mounting medium. The resulting staining was evaluated microscopically (Keyence BZ-X, Keyence Corporation, Osaka, Japan).

As a negative control, one cryo-section was heat-treated at 65 °C for 1 h and subsequently treated with 12% formaldehyde for 15 min, resulting in a complete lack of coloration when NBTC staining was performed.

Statistical analysis

Statistical analysis was performed with GraphPad Prism 10.6.1 (Graphpad Software Inc., Boston, MA, USA). We performed a 2-way ANOVA with Tukey's multiple comparisons test. p values < 0.05 were considered significant.

To evaluate the metabolic tendencies observed in the different systems after irradiation, we calculated the relative change between the treated groups' median values ($M_{irradiated}$) to their corresponding controls ($M_{control}$) according to the following formula:

$$\textbf{\% change} = \frac{(\mathbf{M_{irradiated}} - \mathbf{M_{control}})}{|\mathbf{M_{control}}|} \times \mathbf{100} \quad (4)$$

Negative relative change depicted metabolite decrease in the medium; positive relative changes showed metabolite increase in the medium. A relative difference of $\leq \pm 5\%$ was considered as "no change" (nc).

3. Results

To elaborate on the topic of cross-system reproducibility of UVA-induced metabolic profiles, we concentrated on two main questions. Firstly, what immediate metabolic effects are detectable in vivo after UVA irradiation? Secondly, how do the in vivo acquired metabolic profiles match metabolic profiles obtained in vitro and ex vivo?

3.1. Comparing the Cutaneous Metabolic Profiles of Three Volunteers Before and After UVA1 Irradiation

Via microdialysis, we collected control samples from the probands' skin before irradiation (control). We then compared the acquired metabolic profiles with data obtained during and immediately after UVA1 irradiation of the skin (UVA) (Figure 1). For the 29 metabolites assayed with GC–TOF-MS (Figure 1 and Supplemental Figures S5–S7), the probands showed differential metabolic profiles. Some metabolites, including, among others, alanine, glutamine, and histidine, showed decreased concentrations in the interstitial fluid after UVA irradiation in at least one of the three probands. However, on average, UVA1 irradiation resulted in increased metabolite concentration in the interstitium of all three probands (Figure 1).

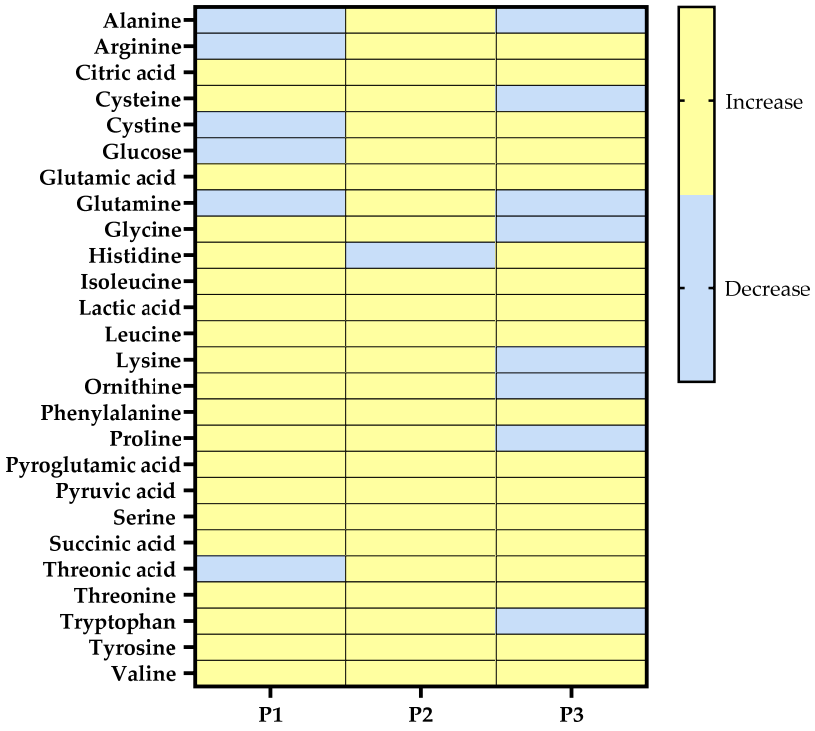

Figure 1. Microdialysis data acquired in vivo from three probands after UVA treatment of the lower arm showing increase (yellow) or decrease (blue) of metabolite concentrations after UVA treatment.

Due to the small number of probands in the in vivo experiment, the values obtained via microdialysis were not a subject of statistical interpretation for the determination of significance. However, the clear fold change increase after irradiation was seen as biologically relevant and used as a guideline to evaluate the cross-system reproducibility of the UVA-induced metabolic changes in the in vivo, in vitro, and ex vivo systems (Figure 2, as well as Supplemental Figures S5–S7).

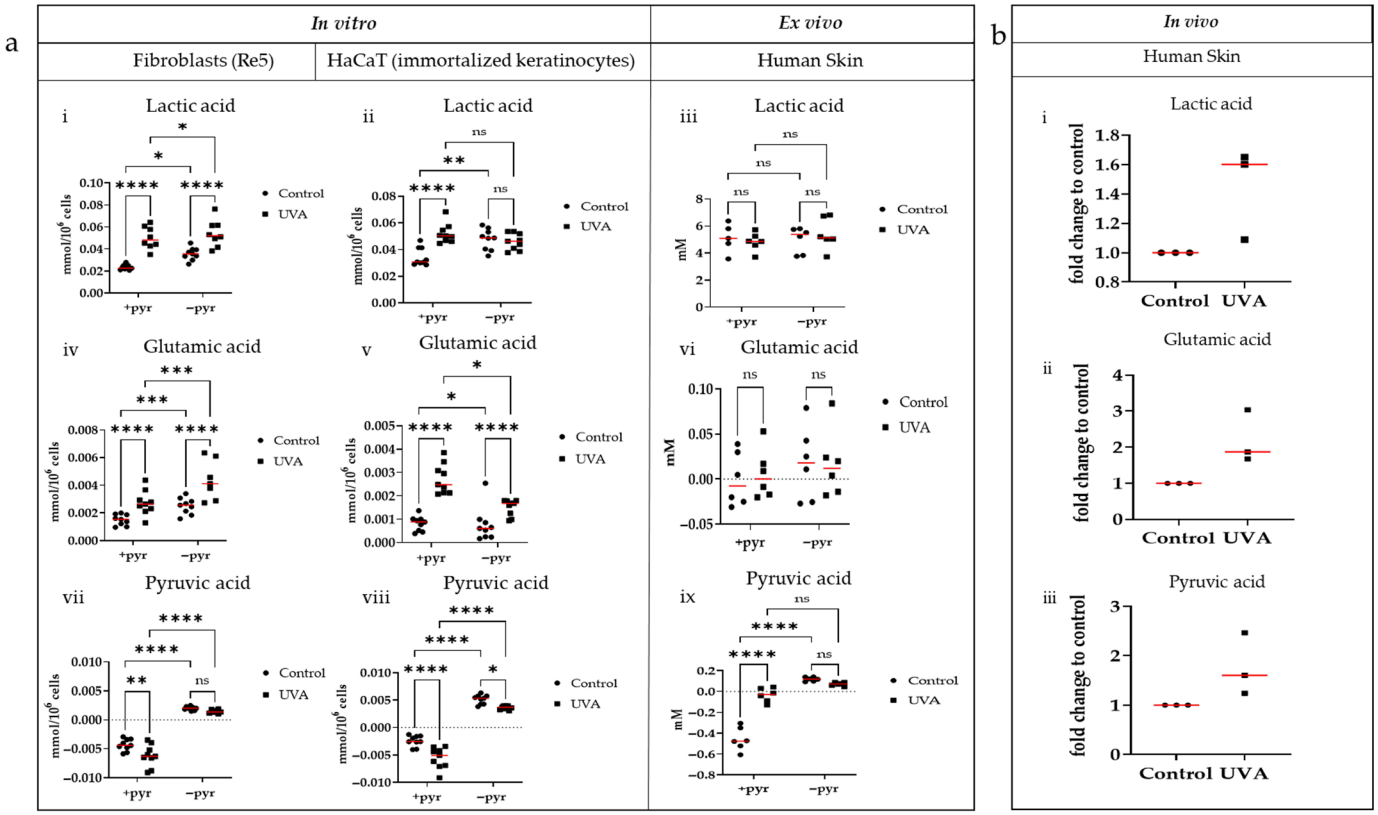

Figure 2. A representative excerpt of the metabolites analyzed, showing the effects of UVA irradiation detected in four different experimental systems—in vitro cell culture (Re 5 and HaCaT), ex vivo skin explants, and in vivo microdialysis. (**a**) (i–iii) Lactic acid, (iv–vi) glutamic acid, and (vii–ix) pyruvic acid changes post irradiation were observed in in vitro cultures of human fibroblasts and HaCaT cells and in ex vivo cultures of human skin explants. (**b**) Fold changes of (i) lactic acid, (ii) glutamic acid, and (iii) pyruvic acid were observed in vivo after UVA treatment. +/− pyr = +/−1 mM pyruvate in the culture mediumpyr 1 mM pyruvate in the culture medium. Statistical analysis: A 2-way ANOVA with Tukey's multiple comparisons test (ns—$p > 0.05$, *—$p \leq 0.05$, **—$p \leq 0.01$, ***—$p \leq 0.001$, ****—$p \leq 0.0001$). Median values for each group are marked in red.

3.2. Comparing the Metabolic Profiles of Lactic Acid, Glutamic Acid, and Pyruvic Acid Between In Vitro, Ex Vivo, and In Vivo Systems

Using the data collected in vivo via microdialysis as a reference point, we investigated the heterogeneity of in vitro and ex vivo culture data and if they mirrored the obtained metabolic profiles. The acquisition of the metabolic profiles for the in vitro and ex vivo cultures was performed via NMR, while the in vivo data were obtained via GC–TOF-MS. Figure 2 shows an excerpt of the metabolic data acquired from our in vitro (human fibroblasts and immortalized keratinocytes), ex vivo (human skin explants), and in vivo systems after UVA1 treatment (for exhaustive data see Supplemental Figures S5–S7). Neither the culturing conditions nor the irradiation regimen negatively influenced the cell and tissue viability (Supplemental Figures S3 and S4, respectively).

Compared to the microdialysis data where irradiation largely resulted in global increases in assayed metabolites, the two artificial systems showed a more diverse reaction to UVA1. The larger sample sets in the in vitro and ex vivo experiments allowed for statistical analysis of the observed metabolic effects in those systems (Figure 2).

In the case of lactic acid, primary human fibroblasts Re5 cultured with or without pyruvate, as well as immortalized keratinocytes (HaCaT) cultured with 1 mM pyruvate, showed an overall increased metabolite accumulation in the culture medium after irradiation. This tendency reflects the metabolic profile observed in human skin in vivo after UVA1 treatment (Figure 2(ai,aii,bi)). The data collected from skin explants (Figure 2(aiii)) did not mirror our in vitro or in vivo data.

Glutamic acid also showed increased concentrations in the culture medium after UV irradiation in Re5 and HaCaT cells (with and without pyruvate) (Figure 2(aiv,av)). In skin explants cultured with pyruvate, the tendency of higher glutamic acid concentrations in the medium post irradiation was also detectable, albeit not statistically significant. Similarly, irradiated human skin in vivo had increased glutamic acid concentrations compared to un-irradiated skin (Figure 2(avi,bii)).

Compared to lactic acid and glutamic acid, pyruvic acid data acquired in vivo differed from the ones observed in vitro. Both Re5 and HaCaT cells cultured with 1 mM pyruvate showed increased pyruvic acid consumption from the medium after irradiation compared to un-irradiated cells. When cultured in the absence of pyruvate (−pyr), both cell lines released pyruvic acid into the medium. Upon irradiation, the pyruvic acid levels in the medium of −pyr cultures decreased compared to untreated samples (Figure 2(avii,aviii)). The ex vivo skin culture (Figure 2(aix)) partially mimicked the in vitro data under culturing conditions without pyruvate. In the case of skin explants cultured with pyruvate, the metabolic profile partially corresponded to the in vivo metabolic data (Figure 2(aix,biii)).

3.3. Comparing the Results of In Vitro and Ex Vivo Metabolic Screenings with the Data Obtained from In Vivo Skin Microdialysis

We extended our comparison between microdialysis and in vitro/ex vivo data to 16 metabolites that were enriched in the interstitium after irradiation (see Figure 3).

In a dynamic system that interacts with blood vessels, an increase in the extracellular metabolic concentrations upon UV treatment could be the result of decreased metabolite consumption or increased release. Therefore, for our static systems (cell culture and skin explants), we equated metabolites showing increased release and decreased consumption to having the same tendency as increased metabolite concentrations in vivo (Figure 3). We then discriminated between metabolites showing similar metabolic trends to the ones observed in vivo and metabolites showing inverse metabolic tendencies. Those two major groups were then subdivided into metabolic changes that were statistically significant and such that showed clear, yet not significant tendencies. A third major group was established for metabolic profiles that showed $\leq \pm 5\%$ relative difference between the UVA-treated median values and their corresponding controls. These profiles were equated to no UVA-induced metabolic changes (white in Figure 3).

For citric acid, isoleucine, leucine, phenylalanine, serine, and valine, in vitro and ex vivo cultures often failed to reproduce the in vivo data (Figure 3, and Supplemental Figures S5–S7). Even in cases where similar tendencies were observed between the proband and culture data, the observed effects of UVA1 irradiation between irradiated and un-irradiated culture samples were not statistically significant.

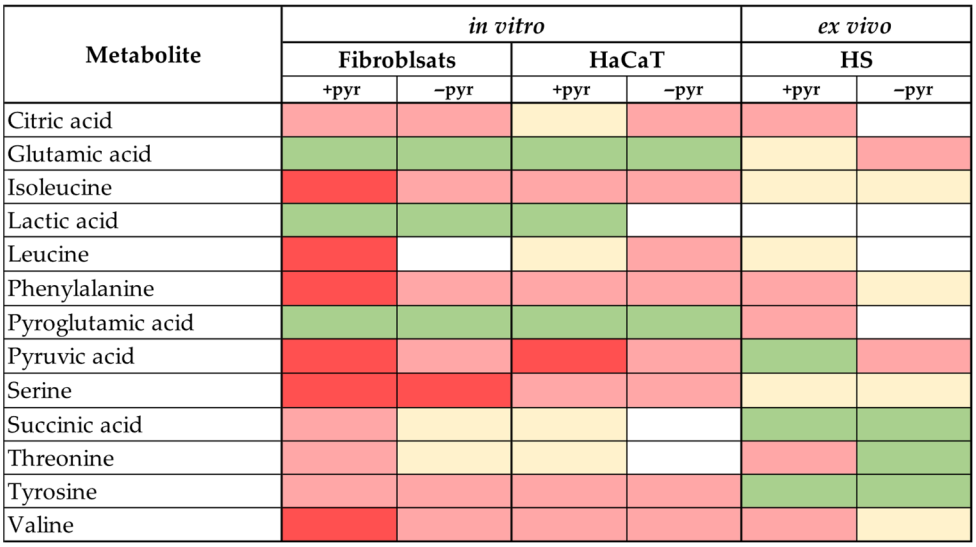

Figure 3. Metabolites showing increased interstitial levels in all 3 probands after irradiation in vivo, compared to irradiated cultured samples. Green—profiles overlap with the in vivo tendencies and show statistically significant UVA influence in the artificial systems. Yellow—profiles overlap with the in vivo tendencies, but the observed tendency is not statistically significant. Red—UVA treatment leads to statistically significant changes in the metabolite profiles that are inverse to the ones observed in vivo. Pink—UVA treatment results in metabolic changes that are inverse, but not statistically significant, to the ones observed in vivo. White—UV treatment resulted in no metabolic changes compared to in vivo (relative difference in the median values between UV and control $\leq \pm 5\%$). Pyr—pyruvate, HS—human skin.

UVA1-induced changes in the profiles of glutamic acid, lactic acid, and pyroglutamic acid observed in vitro in both fibroblast and keratinocyte cultures closely resembled the in vivo data (Figures 2, 3 and S6). For pyruvic acid, succinic acid, threonine, and tyrosine, ex vivo skin culture yielded results most closely correlating with the microdialysis data (Figures 2, 3 and S7).

From all experimental systems, the fibroblasts cultured without pyruvate yielded the highest number of metabolic profiles, showing statistically significant inverse changes compared to in vivo, followed by fibroblasts without pyruvate and HaCaT +pyr cells (Figure 3). This included metabolites such as pyruvic and lactic acids, serine, leucine, isoleucine, and valine.

Both HaCaT −pyr and human skin (HS) −pyr systems yielded a high number of metabolites that showed no UVA-induced changes compared to in vivo.

3.4. Influence of Culture Type and Culture Medium on Data Reproducibility Between In Vitro, Ex Vivo, and In Vivo Systems

As shown in Figure 3, not all UVA1-induced metabolic effects detected in vivo can be observed in different in vitro and ex vivo systems. Since we wanted to concentrate on finding the best artificial system to reproduce UVA-induced metabolic changes observed in vivo, we narrowed the data categories shown in Figure 3 to three—"same", "same (ns)", and "other". Under the umbrella term "other" fell metabolic profiles that were inverse to the ones observed in vivo (both statistically significant and not) and profiles showing no UV-induced changes.

As shown in Table 1, cultures held in media without pyruvate, a condition that should resemble the pyruvate levels detected in blood more closely [27,66], were not inherently better comparable to the in vivo data than cultures held in medium with 1 mM pyruvate (ten times the blood values).

Table 1. Summary of the number of metabolites from each category (same/same (ns)/other †) corresponding to each experimental system.

Matches with In Vivo	In Vitro				Ex Vivo	
	Fibroblasts +pyr	Fibroblasts −pyr	HaCaT +pyr	HaCaT −pyr	HS +pyr	HS −pyr
Same	3	3	3	2	3	3
Same (ns)	0	2	4	0	4	4
Other	10	8	6	11	6	6

† Same—profiles (in vitro and ex vivo) match with tendencies observed in vivo and are statistically significant; Same (ns)—profiles (in vitro and ex vivo) match with tendencies observed in vivo but are not statistically significant; Other—profiles (in vitro and ex vivo) do not match with tendencies observed in vivo (nc, inv, inv (ns)). HS—human skin.

For Re5 fibroblasts cultured in the absence of pyruvate, three out of thirteen metabolites showed similar UVA1-induced metabolic patterns like the microdialysis samples, which were also statistically significant. Two metabolites showed metabolic tendencies after UVA1 irradiation similar to the ones detected in vivo, but the differences between irradiated and un-irradiated samples were not statistically significant (Table 1). Re5 fibroblasts kept with pyruvate performed worse than their counterparts cultured without pyruvate when it came to replicating the in vivo metabolic profile (ten mismatches to the in vivo profiles for cells cultured with pyruvate versus eight mismatches for cells cultured without pyruvate) (Table 1).

HaCaT cultured with pyruvate showed a metabolic profile most similar to the ones observed in vivo. However, they also showed one statistically significant inverse metabolic change compared to in vivo in the case of pyruvic acid (Figure 3). HaCaT cells without pyruvate showed the lowest overlap, with only two out of the thirteen screened metabolites showing similar profiles like the ones detected in vivo. Culturing HaCaT cells with pyruvate yielded better results in terms of matching the in vivo data (only six mismatches compared to eleven mismatches for HaCaT without pyruvate).

For ex vivo skin explant cultures as well, the absence of pyruvate from the system did not result in a closer resemblance of in vivo metabolic profiles. Both HS +pyr and HS −pyr had six of thirteen metabolites showing a mismatch (Table 1). Interestingly, the skin explants showed the same level of congruity with the in vivo data as the HaCaT culture with pyruvate (significant UVA changes in three out of thirteen metabolites and UVA-induced non-significant tendencies in four out of thirteen metabolites). However, it should be noted that the metabolites matching the in vivo situation were different in all three cultures (see Figure 3).

4. Discussion

Being able to acquire reliable and reproducible data on the skin metabolic profile after irradiation is crucial in the field of dermatology. Robust and cheap experimental systems are the key to elucidating the etiology of photosensitive skin diseases, making them the basis for the research of novel and improved therapeutics and anti-aging and sun-protection strategies.

In this study, we looked at the data transferability between different experimental systems (in vitro, ex vivo, in vivo) in the context of UV-induced metabolic changes. From the large pool of available metabolites, we concentrated on small organic acids, especially amino acids. This was due to several factors. Firstly, due to the collection method for the samples (from culture supernatant and microdialysate), we were constrained to metabolites that are well-soluble in aqueous solutions. This is one drawback of using microdialysis

for in vivo metabolic measurements that must be taken into consideration when using this technique. Secondly, from a skin-physiological point of view, the chosen small organic acids are versatile compounds participating in skin repair, acid–base balance, antioxidative defense, and immune response modulation [67–69]. All these functions are crucial for restoring tissue homeostasis after UV irradiation. Lastly, all the chosen compounds are well detectable via NMR and GC–TOF-MS.

Both NMR and GC–TOF-MS are excellent tools for high-throughput testing of multiple samples. Especially when used on aqueous solutions, both methods require minimal sample preparation before measurement. This shortened processing time ensures that the measured metabolic profiles are as close as possible to the true metabolic landscape in the skin. Although we use both metabolite detection platforms interchangeably in this work, it is important to note that each of the methods has its unique strengths and weaknesses. NMR is an excellent tool for exploratory, untargeted metabolomics since it works with native samples without the need for derivatization. It has high reproducibility, and the non-destructive nature of the sample preparation allows multiple measurements of the same sample. However, the sensitivity of NMR is lower, requiring higher metabolite concentrations. On the other hand, GC–TOF-MS is highly sensitive, detecting metabolites in the pico- to femtomolar ranges and working with very small sample volumes. A caveat of the technique is that it requires sample derivatization, thus necessitating beforehand knowledge of the compounds of interest and different chromatographic techniques to assess different classes of metabolites [70,71]. Some metabolites can avoid detection due to their molecular composition, size, or volatility. This makes it necessary to either choose the compounds to be assessed beforehand in accordance with the detection platform available or to apply multiple detection methods on the same sample [72].

In our experimental setup, we relied on both relative and absolute quantification to assess tendencies in metabolic behavior before and after UVA irradiation. We also compared only metabolites that are well detectable with both GC–TOF-MS and NMR, assuring scalability between measurements. We did this with the intention of showing that, under specific experimental conditions and with a good knowledge of the targeted metabolites, one should not feel constrained by the detection platform used.

Looking at our microdialysis data, UVA1 irradiation induced a global increase in metabolite concentration in the cutaneous interstitium. It should be acknowledged that the number of probands needs to be increased in order to achieve a more reliable conclusion. Thus, the in vivo results acquired in this experiment were used mainly as qualitative reverence for cross-system comparison. Still, the fact that the observed metabolic reactions post irradiation in all three probands were similar, despite their differences in age, gender, and genetic background, points towards an orchestrated metabolic response to UVR stimulation of the skin. It should be noted that the increase in metabolic concentrations post UVA1 irradiation could be triggered by the dilatation of skin-supplying blood vessels [73]. However, several different metabolites amongst the three probands showed a decrease in abundance after irradiation, which suggests a UVA1-dependent metabolic regulation irrespective of vasodilation.

Further comparing our in vitro and ex vivo models, it was the ex vivo skin explants that showed the highest congruence with the in vivo data. Between the two different pyruvate formulations (+pyr/−pyr) the skin explant culture allowed for the detection of significant metabolic changes in four out of thirteen assayed metabolites. It also allowed the observation of metabolic tendencies (not significant) correlating with the in vivo profile for an additional six (6) metabolites. Still, this finding was surprising since we expected a higher overlap between ex vivo skin explants and the in vivo data. The native ECM's complex three-dimensional structure and the diverse cell populations in skin explants

should make human explant culture without pyruvate the preferred system for studying UVA-induced skin metabolic effects. Additionally, the concentration of blood pyruvate in humans is around 80–100 μM [74,75], and there is a linear correlation between blood and skin pyruvate levels [55]. Thus, considering the ability of cultured cells to equilibrate their medium pyruvate levels to physiological levels [27], an ex vivo skin system without pyruvate should be closer to the natural extracellular conditions than one containing 1 mM pyruvate (standard DMEM formulation). We thus expected the system without pyruvate to yield data more closely matching the in vivo results; however, our expectation was not confirmed. Furthermore, as illustrated in Figure 3, the UVA-induced changes in the concentrations of several key metabolites could not be reliably depicted by the human skin explants but rather in cell culture.

For example, citric acid (citrate) concentration correlated with the in vivo data only when assayed in the supernatant of HaCaT cells cultured with pyruvate (Figures 3 and S5). There, we observed an increased citric acid release after irradiation. As an intermediate of the tricarboxylic acid (TCA) cycle, extracellular citric acid can be used by the cells as an additional source of energy during cellular respiration [76]. Hornig-Do and associates showed that compared to fibroblasts, keratinocytes have difficulty accelerating mitochondrial oxidation in the presence of substrates that feed into the respiratory chain [77]. Although in their experiments they used malate and pyruvate as electron donors for Complex I, it is not unlikely that extracellular citrate can experience a similar fate under high-pyruvate conditions. In media with abundant pyruvate, a precursor to citrate [78], and under the oxidative stress conditions provided by UVA1 [79], inefficient respiration or oxidative damage to TCA enzymes could result in decreased consumption of medium citrate and even its release by the cells in the extracellular milieu. The fact that the skin explant culture, containing both fibroblasts and keratinocytes, showed UVA-induced changes in citrate metabolism, which differed starkly from the in vivo data, remains to be elucidated.

Besides citric acid, other organic acids assayed in this work are a further example of the need for a metabolite-by-metabolite assessment when choosing the optimal experimental system for studying UVA-induced metabolic changes in the skin. In our experiments, glutamic, lactic, and pyroglutamic acids showed UVA profiles closest to the in vivo data when assayed via an in vitro cell culture environment. Pyruvic and succinic acids, on the other hand, showed better agreement when tested in skin explant culture.

In the case of lactic acid (lactate), it can be retained in the ECM of the skin [80]. This explains the unreliable detection of UVA-induced changes in lactate concentration from the culturing medium of skin explants but not in monolayer cell cultures.

The behavior of pyruvate (pyruvic acid) in the different systems is, to a certain extent, connected to the changes in lactate levels. As depicted in Figure 2, we can observe that after UVA irradiation the increase in lactate production correlated with increased pyruvate depletion from the medium (in vitro cultures +pyr). In contrast, in vitro cultures –pyr showed decreased pyruvate release with increasing lactate levels. As noted by O'Donnel-Tormey, cells cultured without pyruvate attempt to equilibrate to physiological pyruvate conditions [27], which we observed in our in vitro cultures (−pyr). Further, pyruvate can non-enzymatically decarboxylate to acetate, especially under high reactive oxygen species (ROS) concentrations [1,28]. Therefore, a reduction in pyruvate release in the culture medium after irradiation is not surprising, especially in a system lacking fresh pyruvate supplementation via the blood flow (cell cultures –pyr). Since pyruvate can quench UVA-induced ROS [1,28,81] and can be used as an additional energy source [82], it is not surprising that in a culture system with abundant medium pyruvate (cell culture +pyr), UVA irradiation leads to increased metabolite consumption.

Skin explant cultures –pyr, similar to the in vitro systems, also showed a decrease in pyruvate release upon irradiation. Their stable lactate levels could be, as mentioned, a result of ECM retention of lactate [80]. In the case of skin explant cultures +pyr, however, there is a decrease in pyruvate consumption from the medium and even a slight release. This tendency is somewhat similar to the effects observed in intact skin after UVA irradiation, showing increased pyruvate levels in the interstitium. Considering the sponge-like ability of the ECM to trap lactate [80], it is possible that a local accumulation of lactate in combination with already abundant extracellular pyruvate influences the diffusion of pyruvate through the ECM and/or its uptake by the cells. Further studies are needed to elaborate on the exact mechanisms behind such behavior.

The fact that changes in succinate (succinic acid) levels after UVA irradiation detected in skin explants were closer to the ones observed in vivo, compared to the cell culture data, is not surprising. Succinate has been shown to accumulate in adipose tissue and be released under hypoxic conditions [83,84]. Although the subcutaneous fat was removed as best as possible from the skin punches before culturing them, residual fat cells could have contributed to the succinate pool in the system.

In the case of glutamate (glutamic acid) and pyroglutamate (pyroglutamic acid), their metabolic profiles after UVA irradiation in vitro closely matched the in vivo data. Ex vivo culture data were not comparable with the in vivo results. A plausible explanation for the lack of glutamate and pyroglutamate secretion in the culture medium of the skin explants is the retention of these two metabolites in the ECM. Glutamate is known to be a paracrine signaling molecule in the skin [85,86]. Its retention in close proximity to its target cells by a complex sponge-like structure, such as the ECM, is not unlikely. The behavior of glutamate after UVA irradiation in vivo is more closely mirrored by our cell culture systems than by the skin explants. Pyroglutamate is part of glutathione metabolism and is often a marker of metabolic and oxidative stress [87,88]. This supports our cell culture findings and in vivo data, showing increased pyroglutamate levels after UVA irradiation in the cell culture medium and the interstitial fluid. However, irradiating skin explants did not result in pyroglutamate release but rather its consumption from the medium. Since pyroglutamate can originate from the spontaneous cyclisation of glutamate, its availability in the culture medium is not surprising. The lack of increased medium pyroglutamate level for the skin explants after irradiation, however, was unexpected, pointing to a possible metabolite retention by the skin explant. This behavior was similar to that observed for lactate, glutamate, and partially pyruvate. Furthermore, lactate is capable of remodeling the ECM by facilitating collagen production and matrix metalloproteinase (MMP) activation [5,89]. It is possible that lactate-triggered changes after UV irradiation contribute to changes in the ECM that promote a selective retention of metabolites. Further studies are needed to elaborate on the exact structural and biochemical modifications responsible for this phenomenon.

When studying skin-relevant organic acids, we therefore recommend using cell cultures to detect UVA-induced changes in glutamic, lactic, citric, and pyroglutamic acids, and skin explant systems for succinic and pyruvic acids when microdialysis is not an option.

The skin explant system without pyruvate can further be useful for studying UVA-induced changes in valine, serine, phenylalanine, and isoleucine, if skin microdialysis is not feasible. Still, an optimization of the culturing conditions needs to be performed in order to achieve optimal results. In the case of leucine, a HaCaT culture +pyr appears to be the most cost-effective alternative system to in vivo approaches.

Ex vivo cultures without pyruvate also seem to be a good alternative for studying threonine and tyrosine. Compared to cell culture, skin explant culture yielded more homogeneous data with less sample variation. This could be explained by the functions

of threonine and tyrosine in the skin. Threonine is a key amino acid in collagen synthesis. It is responsible for stabilizing the helical structure of collagen [90]. In a collagen-rich environment such as the skin ECM, UVA-induced activation of MMPs [1] could lead to the enrichment and release of free threonine in the culture medium, as observed in our study. On the other hand, tyrosine is a substrate for melanogenesis [91–93] and thus more abundant in melanocyte-containing skin explants than in the fibroblasts and keratinocytes monocultures.

A summary of the advantages and disadvantages of the individual approaches is depicted in Figure 4. Among them, the biggest limitation for experimental setups using in vivo microdialysis and ex vivo skin, besides ethical concerns and patient variability, is the probands acquisition, resulting in small sample sizes and challenging statistical interpretation of the data. For microdialysis, small sample volumes and long collection times can be a deterring factor for choosing the technique.

Experimental system	Pros	Cons	Conclusions from the current work
***In vivo* microdialysis** 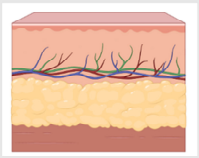	- Represents the state of the skin - Most exact depiction of interactions in a complex, dynamic environment - Allows metabolite detection in short time ranges	- Expensive - Difficult probands recruitment - Ethical considerations - Requires highly specialized personnel - Not suitable for long-term experiments - External influences (age, sex, diet) on experimental outcome - Low material yield - High donor-heterogeneity	- Provides good insight in short-term influences of UVA on the skin. - Allows monitoring of metabolic changes in small time increments
***Ex vivo* skin explants** 	- Inexpensive - Scalable - Moderate material yield - Complex 3D structure - Variety of cells	- Donor-heterogeneity - Not suitable for long-term experiments - More difficult to obtain and maintain - Metabolite concentration over time needed for proper detection - Ethical considerations	- Closest to the in vivo system in terms of detectable UVA-induced metabolic effects - Good for analyzing metabolites that are derived from ECM components, fat tissue, or melanogenesis
***In vitro* cell culture** 	- Inexpensive - Scalable - Reproducible - High material yield	- Overly simplified - 2D structure - Single cell type - Metabolite concentration over time needed for proper detection - Different UV sensitivity compared to *in vivo* skin	- Good for detecting organic acids and metabolites that can be retained in the ECM

Figure 4. Summary of the experimental results and discussion of pros and cons of each tested experimental system.

On the other hand, in vitro cell cultures with their reproducibility, simple sample acquisition, and low costs are tempting and often a viable representation of the metabolic processes in the skin. However, their different sensitivity to UV irradiation compared to intact skin, their monocellular nature, and the big medium influences on their behavior are points that need to be taken into consideration.

It should be noted that the detected metabolic changes in this work are a result of the chosen experimental systems and irradiation regimens and could differ with different types of cells, irradiation treatments, and irradiation wavelengths.

We chose to compare primary fibroblasts with HaCaT cells due to the medium compatibility between the two cultures. Primary isolates, although a more accurate representation of the skin cell population, often come with the caveat of needing special culturing media,

as in the case of primary keratinocytes. Weighing the advantages of having a uniform and easily comparable medium between different experimental systems and the disadvantages stemming from using immortalized cell lines [94] should be taken into consideration during experimental planning. In the case of this study, we believe that HaCaT still remains a good representation of the keratinocyte reaction to UVA treatment, considering its history as a model system for UV-induced metabolic changes [95–98].

In the current work, we also applied different irradiation regiments between in vitro, ex vivo, and in vivo systems. By doing so, we attempted to compensate for differences in prior UV exposure between systems and reduce tissue and cellular damage. The human skin is subject to regular UV irradiation via sun exposure and is thus UV-primed. Therefore, a singular, high dose of UVA would be less damaging in vivo than in artificial systems. Additionally, not every area of the body receives an equal amount of solar irradiation [99]. The ex vivo skin explants for our experiments come from abdominal flaps that are less sun-exposed than the lower arm used for microdialysis. Intuitively, one might choose a singular, yet lower dose of irradiation in an attempt to mimic the in vivo results. However, the fact that the explant culture is separated from the blood flow and experiences nutritional stress and diminished viability should be taken into consideration [59]. A milder, repetitive low-dose treatment is better to ensure skin viability. In addition, the repetitive irradiations mimic a chronic exposure to UVA, which compensates for potential differences in UV priming between the different tissues and thus results in an overall metabolic response closer to in vivo than a singular high dose of UVA. Compared to skin explants, monolayer cultures have easier access to nutrients via diffusion, but are more susceptible to UV damage due to the lack of stratum corneum protection [100]. Additionally, cells in culture have no exposure to UV prior to experimentation. All this needs to be taken into consideration during the experimental planning. In this study, we chose repetitive, low-dose irradiation for our in vitro cultures to minimize UV damage. Furthermore, to compensate for the UV exposure differences compared to the skin, the cultured cells were given a longer irradiation regimen compared to ex vivo samples. Short-term treatments carry the danger of not eliciting enough UV priming to be comparable to the skin explants, and even less to the chronically sun-exposed skin in vivo. Thus, prolonged treatment better mimics the in vivo sun exposure and yields comparable metabolic profiles throughout the different experimental systems.

5. Conclusions

With UV-induced metabolic profiles vastly varying between in vivo, ex vivo, and in vitro systems, our findings emphasize the need for an individual, metabolite-by-metabolite approach when deciding on the proper experimental setup to perform UVA irradiation experiments with regard to cutaneous physiology. Such an individualistic approach will allow for achieving optimal results with the least amount of cost and time, paired with maximal data reproducibility and reliability.

Supplementary Materials: The following supporting information can be downloaded at https://www.mdpi.com/article/10.3390/metabo16020102/s1, Figure S1: Graphical representation of in vitro and ex vivo irradiation regiments; Figure S2: Graphical representation of in vivo irradiation regiments; Figure S3: Viability of Re5 and HaCaT cells after irradiation, measured with Luna FL; Figure S4: NBTC viability assay of skin explants; Figure S5: Metabolic analysis of citrate, isoleucine, and leucine in the presence and absence of pyruvate; Figure S6: Metabolic analysis of phenylalanine, pyroglutamate, and serine in the presence and absence of pyruvate; Figure S7: Metabolic analysis of succinate, threonine, tyrosine, and valine in the presence and absence of pyruvate.

Author Contributions: Conceptualization, I.I., B.K., and Y.K.; methodology, I.I., W.G., A.E., and B.K.; formal analysis, I.I.; data curation, I.I.; investigation, I.I., T.S., W.G., M.L., and B.K.; resources, M.B., A.E., L.P., M.L., and W.G.; writing—original draft preparation, I.I., D.N., B.K., M.L., T.M., W.G., and T.S.; writing—review and editing, I.I., T.S., T.M., and D.N.; visualization, I.I.; supervision, Y.K., B.K., and M.B.; project administration, B.K. and Y.K.; funding acquisition, Y.K. and M.B. All authors have read and agreed to the published version of the manuscript.

Funding: This work was partially funded by the ANR DFG Number (BE 2005/8-1).

Institutional Review Board Statement: The study was conducted in accordance with the Declaration of Helsinki. All microdialysis experiments were approved by the Institutional Review Board of the University of Regensburg, Germany (Permit Number: 22-3065-101, Approval date: 21 September 2022). The collection and propagation of primary human fibroblasts was approved by the Institutional Review Board of University of Regensburg (Permit Number: 14101 0001). Human skin from three volunteers was acquired from the Department of Plastic Surgery in accordance with the Institutional Review Board of the University of Regensburg, Germany (Permit Number: 23-3484-101).

Informed Consent Statement: Informed consent was obtained from all subjects involved in the study.

Data Availability Statement: Detailed information about materials, methods, and data are available upon request.

Conflicts of Interest: Dennis Niebel reports a relationship with the following: AbbVie Inc. that includes consulting or advisory, speaking and lecture fees, and travel reimbursement; Apogee Therapeutics Inc. that includes consulting or advisory; Boehringer Ingelheim GmbH that includes consulting or advisory and speaking and lecture fees; Bristol Myers Squibb Co that includes consulting or advisory; Almirall SA that includes consulting or advisory, speaking and lecture fees, and travel reimbursement; Eli Lilly that includes consulting or advisory and speaking and lecture fees; Hexal AG that includes speaking and lecture fees; Incyte Corporation that includes consulting or advisory and speaking and lecture fees; Johnson & Johnson Services Inc. that includes consulting or advisory and speaking and lecture fees; LEO Pharma that includes consulting or advisory and speaking and lecture fees; Novartis that includes consulting or advisory and speaking and lecture fees; Pfizer that includes speaking and lecture fees; Regeneron GmbH that includes speaking and lecture fees; Sanofi-Aventis Deutschland GmbH that includes consulting or advisory and speaking and lecture fees; UCB Pharma GmbH that includes consulting or advisory and speaking and lecture fees. The funders had no role in the design of the study; in the collection, analyses, or interpretation of data; in the writing of the manuscript; or in the decision to publish the results. All other authors declare that they have no known competing financial interests or personal relationships that could have appeared to influence the work reported in this paper.

Abbreviations

The following abbreviations are used in this manuscript:

BSTFA	N,O-Bis[trimethylsilyl]trifluoroacetamide
CPMG	Carr-Purcell-Meiboom-Gill
DMEM	Dulbecco's Modified Eagle Medium
ECM	Extracellular matrix
FCS	Fetal calf serum
GC–TOF-MS	Gas chromatography coupled to time-of-flight mass spectrometry
HS	Human skin
MED	Minimal erythema dose
MMP	Matrix metalloproteinase
NBTC	Nitroblue tetrazolium chloride
NMR	Nuclear magnetic resonance
PBS	Phosphate-buffered saline

pyr	Pyruvate
ROS	Reactive oxygen species
TCA	Tricarboxylic acid
UV	Ultraviolet

References

1. Ivanova, I.; Bogner, C.; Gronwald, W.; Kreutz, M.; Kurz, B.; Maisch, T.; Kamenisch, Y.; Berneburg, M. UVA-induced metabolic changes in non-malignant skin cells and the potential role of pyruvate as antioxidant. *Photochem. Photobiol. Sci.* **2023**, *22*, 1889–1899. [CrossRef]
2. Kremslehner, C.; Miller, A.; Nica, R.; Nagelreiter, I.-M.; Narzt, M.-S.; Golabi, B.; Vorstandlechner, V.; Mildner, M.; Lachner, J.; Tschachler, E.; et al. Imaging of metabolic activity adaptations to UV stress, drugs and differentiation at cellular resolution in skin and skin equivalents—Implications for oxidative UV damage. *Redox Biol.* **2020**, *37*, 101583. [CrossRef]
3. Dayan, A. Solar and ultraviolet radiation. IARC monographs on the evaluation of carcinogenic risks to humans. Vol 55. *J. Clin. Pathol.* **1993**, *46*, 880. [CrossRef]
4. Lyon, F. *IARC Monographs on the Evaluation of Carcinogenic Risks to Humans*; World Health Organization, International Agency for Research on Cancer: Lyon, France, 2014.
5. Barba, F.J.; Roohinejad, S.; Ishikawa, K.; Leong, S.Y.; A Bekhit, A.E.-D.; Saraiva, J.A.; Lebovka, N. Electron spin resonance as a tool to monitor the influence of novel processing technologies on food properties. *Trends Food Sci. Technol.* **2020**, *100*, 77–87. [CrossRef]
6. Kamenisch, Y.; Baban, T.S.; Schuller, W.; von Thaler, A.-K.; Sinnberg, T.; Metzler, G.; Bauer, J.; Schittek, B.; Garbe, C.; Rocken, M.; et al. UVA-Irradiation Induces Melanoma Invasion via the Enhanced Warburg Effect. *J. Investig. Dermatol.* **2016**, *136*, 1866–1875. [CrossRef]
7. Brand, A.; Singer, K.; Koehl, G.E.; Kolitzus, M.; Schoenhammer, G.; Thiel, A.; Matos, C.; Bruss, C.; Klobuch, S.; Peter, K.; et al. LDHA-Associated Lactic Acid Production Blunts Tumor Immunosurveillance by T and NK Cells. *Cell Metab.* **2016**, *24*, 657–671. [CrossRef]
8. Fatima, F.; Das, A.; Kumar, P.; Datta, D. Skin and Metabolic Syndrome: An Evidence Based Comprehensive Review. *Indian J. Dermatol.* **2021**, *66*, 302–307. [CrossRef] [PubMed]
9. Hu, Y.; Zhu, Y.; Lian, N.; Chen, M.; Bartke, A.; Yuan, R. Metabolic Syndrome and Skin Diseases. *Front. Endocrinol.* **2019**, *10*, 788. [CrossRef] [PubMed]
10. Ma, J.; Liu, M.; Wang, Y.; Xin, C.; Zhang, H.; Chen, S.; Zheng, X.; Zhang, X.; Xiao, F.; Yang, S. Quantitative proteomics analysis of young and elderly skin with DIA mass spectrometry reveals new skin aging-related proteins. *Aging* **2020**, *12*, 13529–13554. [CrossRef] [PubMed]
11. Proksch, E.; Schunck, M.; Zague, V.; Segger, D.; Degwert, J.; Oesser, S. Oral intake of specific bioactive collagen peptides reduces skin wrinkles and increases dermal matrix synthesis. *Skin. Pharmacol. Physiol.* **2014**, *27*, 113–119. [CrossRef]
12. Cibrian, D.; de la Fuente, H.; Sánchez-Madrid, F. Metabolic Pathways That Control Skin Homeostasis and Inflammation. *Trends Mol. Med.* **2020**, *26*, 975–986. [CrossRef]
13. Kotronoulas, A.; de Lomana, A.L.G.; Einarsdóttir, H.K.; Kjartansson, H.; Stone, R.; Rolfsson, Ó. Fish Skin Grafts Affect Adenosine and Methionine Metabolism during Burn Wound Healing. *Antioxidants* **2023**, *12*, 2076. [CrossRef] [PubMed]
14. Elpa, D.P.; Chiu, H.-Y.; Wu, S.-P.; Urban, P.L. Skin Metabolomics. *Trends Endocrinol. Metab.* **2021**, *32*, 66–75. [CrossRef]
15. Lei, B.U.W.; Prow, T.W. A review of microsampling techniques and their social impact. *Biomed. Microdevices* **2019**, *21*, 81. [CrossRef]
16. Baumann, K.Y.; Church, M.K.; Clough, G.F.; Quist, S.R.; Schmelz, M.; Skov, P.S.; Anderson, C.D.; Tannert, L.K.; Giménez-Arnau, A.M.; Frischbutter, S.; et al. Skin microdialysis: Methods, applications and future opportunities—An EAACI position paper. *Clin. Transl. Allergy* **2019**, *9*, 24. [CrossRef]
17. Fröhlich, E.; Salar-Behzadi, S. Toxicological Assessment of Inhaled Nanoparticles: Role of in Vivo, ex Vivo, in Vitro, and in Silico Studies. *Int. J. Mol. Sci.* **2014**, *15*, 4795–4822. [CrossRef]
18. National Research Council (US) Committee on Methods of Producing Monoclonal Antibodies. Summary of Advantages and Disadvantages of in vitro and in vivo methods. In *Monoclonal Antibody Production*; National Academies Press: Washington, DC, USA, 1999; pp. 22–24.
19. Saeidnia, S.; Manayi, A.; Abdollahi, M. From in vitro Experiments to in vivo and Clinical Studies; Pros and Cons. *Curr. Drug Discov. Technol.* **2015**, *12*, 218–224. [CrossRef]
20. Quantin, P.; Stricher, M.; Catoire, S.; Ficheux, H.; Egles, C. Dermatokinetics: Advances and Experimental Models, Focus on Skin Metabolism. *Curr. Drug Metab.* **2022**, *23*, 340–354. [CrossRef] [PubMed]
21. Lee, S.-J.; Lee, H.-A. Trends in the development of human stem cell-based non-animal drug testing models. *Korean J. Physiol. Pharmacol.* **2020**, *24*, 441–452. [CrossRef] [PubMed]
22. Eberlin, S.; da Silva, M.S.; Facchini, G.; da Silva, G.H.; Pinheiro, A.L.T.A.; Pinheiro, A.d.S. The Ex Vivo Skin Model as an Alternative Tool for the Efficacy and Safety Evaluation of Topical Products. *Altern. Lab. Anim.* **2020**, *48*, 10–22. [CrossRef]

23. Neves, L.M.G.; Wilgus, T.A.; Bayat, A. In Vitro, Ex Vivo, and In Vivo Approaches for Investigation of Skin Scarring: Human and Animal Models. *Adv. Wound Care* **2021**, *12*, 97–116. [CrossRef]
24. Ghosh, K.; Pan, Z.; Guan, E.; Ge, S.; Liu, Y.; Nakamura, T.; Ren, X.-D.; Rafailovich, M.; Clark, R.A. Cell adaptation to a physiologically relevant ECM mimic with different viscoelastic properties. *Biomaterials* **2007**, *28*, 671–679. [CrossRef]
25. Babich, H.; Liebling, E.J.; Burger, R.F.; Zuckerbraun, H.L.; Schuck, A.G. Choice of DMEM, formulated with or without pyruvate, plays an important role in assessing the in vitro cytotoxicity of oxidants and prooxidant nutraceuticals. *In Vitro Cell. Dev. Biol. Anim.* **2009**, *45*, 226–233. [CrossRef] [PubMed]
26. Olar, T.T.; Potts, A.S. Effects of medium composition on murine and human blastocyst formation and hatching rate. *J. Assist. Reprod. Genet.* **1993**, *10*, 192–196. [CrossRef]
27. O'Donnell-Tormey, J.; Nathan, C.F.; Lanks, K.; DeBoer, C.J.; de la Harpe, J. Secretion of pyruvate. An antioxidant defense of mammalian cells. *J. Exp. Med.* **1987**, *165*, 500–514. [CrossRef]
28. Constantopoulos, G.; Barranger, J.A. Nonenzymatic decarboxylation of pyruvate. *Anal. Biochem.* **1984**, *139*, 353–358. [CrossRef] [PubMed]
29. Kolundzic, N.; Khurana, P.; Crumrine, D.; Celli, A.; Mauro, T.M.; Ilic, D. Epidermal Basement Membrane Substitutes for Bioengineering of Human Epidermal Equivalents. *JID Innov.* **2022**, *2*, 100083. [CrossRef] [PubMed]
30. Atwood, S.X.; Plikus, M.V. Fostering a healthy culture: Biological relevance of in vitro and ex vivo skin models. *Exp. Dermatol.* **2021**, *30*, 298–303. [CrossRef]
31. Hofmann, E.; Schwarz, A.; Fink, J.; Kamolz, L.-P.; Kotzbeck, P. Modelling the Complexity of Human Skin In Vitro. *Biomedicines* **2023**, *11*, 794. [CrossRef]
32. Hruza, L.L.; Pentland, A.P. Mechanisms of UV-Induced Inflammation. *J. Investig. Dermatol.* **1993**, *100*, S35–S41. [CrossRef]
33. Losada-Fernández, I.; Martín, A.S.; Moreno-Nombela, S.; Suárez-Cabrera, L.; Valencia, L.; Pérez-Aciego, P.; Velasco, D. In Vitro Skin Models for Skin Sensitisation: Challenges and Future Directions. *Cosmetics* **2025**, *12*, 173. [CrossRef]
34. Tfayli, A.; Bonnier, F.; Farhane, Z.; Libong, D.; Byrne, H.J.; Baillet-Guffroy, A. Comparison of structure and organization of cutaneous lipids in a reconstructed skin model and human skin: Spectroscopic imaging and chromatographic profiling. *Exp. Dermatol.* **2014**, *23*, 441–443. [CrossRef] [PubMed]
35. Battie, C.; Verschoore, M. Cutaneous solar ultraviolet exposure and clinical aspects of photodamage. *Indian J. Dermatol. Venereol. Leprol.* **2012**, *78*, S9–S14. [CrossRef] [PubMed]
36. Quílez, C.; Bebiano, L.B.; Jones, E.; Maver, U.; Meesters, L.; Parzymies, P.; Petiot, E.; Rikken, G.; Risueño, I.; Zaidi, H.; et al. Targeting the Complexity of In Vitro Skin Models: A Review of Cutting-Edge Developments. *J. Investig. Dermatol.* **2024**, *144*, 2650–2670. [CrossRef]
37. Choudhury, S.; Das, A. Advances in generation of three-dimensional skin equivalents: Pre-clinical studies to clinical therapies. *Cytotherapy* **2021**, *23*, 1–9. [CrossRef]
38. Wurbs, A.; Karner, C.; Vejzovic, D.; Singer, G.; Pichler, M.; Liegl-Atzwanger, B.; Rinner, B. A human ex vivo skin model breaking boundaries. *Sci. Rep.* **2024**, *14*, 24054. [CrossRef]
39. Monteiro-Riviere, N.A.; Inman, A.O.; Snider, T.H.; Blank, J.A.; Hobson, D.W. Comparison of an in vitro skin model to normal human skin for dermatological research. *Microsc. Res. Tech.* **1997**, *37*, 172–179. [CrossRef]
40. Zhou, L.; Ji, W.; Dicolandrea, T.; Finlay, D.; Supp, D.; Boyce, S.; Wei, K.; Kadekaro, A.L.; Zhang, Y. An improved human skin explant culture method for testing and assessing personal care products. *J. Cosmet. Dermatol.* **2023**, *22*, 1585–1594. [CrossRef]
41. Cullati, S.; Courvoisier, D.S.; Gayet-Ageron, A.; Haller, G.; Irion, O.; Agoritsas, T.; Rudaz, S.; Perneger, T.V. Patient enrollment and logistical problems top the list of difficulties in clinical research: A cross-sectional survey. *BMC Med. Res. Methodol.* **2016**, *16*, 50. [CrossRef]
42. Greene, N.M. Metabolic Effects of Anesthetics. In *Modern Inhalation Anesthetics*; Chenoweth, M.B., Ed.; Springer: Berlin/Heidelberg, Germany, 1972; pp. 271–287.
43. Schlosser, S.; Spanholtz, T.; Merz, K.; Dennler, C.; Banic, A.; Erni, D.; Plock, J.A. The Choice of Anesthesia Influences Oxidative Energy Metabolism and Tissue Survival in Critically Ischemic Murine Skin. *J. Surg. Res.* **2010**, *162*, 308–313. [CrossRef]
44. Tan, X.; Liu, R.; Dan, L.; Huang, H.; Duan, C. Effects of anesthetics on mitochondrial quality control: Mechanisms and clinical implications. *Anesthesiol. Perioper. Sci.* **2024**, *2*, 31. [CrossRef]
45. Demetrius, L. Of mice and men. When it comes to studying ageing and the means to slow it down, mice are not just small humans. *EMBO Rep.* **2005**, *6*, S39–S44. [CrossRef]
46. Géniès, C.; Jamin, E.L.; Debrauwer, L.; Zalko, D.; Person, E.N.; Eilstein, J.; Grégoire, S.; Schepky, A.; Lange, D.; Ellison, C.; et al. Comparison of the metabolism of 10 chemicals in human and pig skin explants. *J. Appl. Toxicol.* **2019**, *39*, 385–397. [CrossRef]
47. Otberg, N.; Richter, H.; Schaefer, H.; Blume-Peytavi, U.; Sterry, W.; Lademann, J. Variations of hair follicle size and distribution in different body sites. *J. Investig. Dermatol.* **2004**, *122*, 14–19. [CrossRef] [PubMed]
48. Pomaville, M.B.; Wright, K.M. Follicle-innervating Aδ-low threshold mechanoreceptive neurons form receptive fields through homotypic competition. *Neural Dev.* **2023**, *18*, 2. [CrossRef] [PubMed]

49. Ye, H.; Rinkevich, Y. Fascia Layer—A Novel Target for the Application of Biomaterials in Skin Wound Healing. *Int. J. Mol. Sci.* **2023**, *24*, 2936. [CrossRef]
50. Rittié, L. Cellular mechanisms of skin repair in humans and other mammals. *J. Cell Commun. Signal.* **2016**, *10*, 103–120. [CrossRef]
51. Iyengar, B. The hair follicle: A specialised UV receptor in the human skin? *Biol. Signals Recept.* **1998**, *7*, 188–194. [CrossRef] [PubMed]
52. Benavides, F.; Oberyszyn, T.M.; VanBuskirk, A.M.; Reeve, V.E.; Kusewitt, D.F. The hairless mouse in skin research. *J. Dermatol. Sci.* **2009**, *53*, 10–18. [CrossRef]
53. Waterston, K.; Naysmith, L.; Rees, J.L. Physiological variation in the erythemal response to ultraviolet radiation and photoadaptation. *J. Investig. Dermatol.* **2004**, *123*, 958–964. [CrossRef]
54. Clough, G.F.; Jackson, C.L.; Lee, J.J.; Jamal, S.C.; Church, M.K. What can microdialysis tell us about the temporal and spatial generation of cytokines in allergen-induced responses in human skin in vivo? *J. Investig. Dermatol.* **2007**, *127*, 2799–2806. [CrossRef]
55. Oharazawa, A.; Maimaituxun, G.; Watanabe, K.; Nishiyasu, T.; Fujii, N. Metabolome analyses of skin dialysate: Insights into skin interstitial fluid biomarkers. *J. Dermatol. Sci.* **2024**, *114*, 141–147. [CrossRef] [PubMed]
56. Islam, R.K.; Tong, V.T.; Robicheaux, C.; Tageant, H.; Haas, C.J.; Kline, R.J.; Islam, K.N. The Impact of Anesthesia on Dermatological Outcomes: A Narrative Review. *Cureus* **2024**, *16*, e72321. [CrossRef]
57. Anderson, C.; Andersson, T.; Andersson, R.G. In vivo microdialysis estimation of histamine in human skin. *Ski. Pharmacol.* **1992**, *5*, 177–183. [CrossRef]
58. Anderson, C.; Andersson, T.; Wårdell, K. Changes in skin circulation after insertion of a microdialysis probe visualized by laser Doppler perfusion imaging. *J. Investig. Dermatol.* **1994**, *102*, 807–811. [CrossRef]
59. Ng, K.W.; Pearton, M.; Coulman, S.; Anstey, A.; Gateley, C.; Morrissey, A.; Allender, C.; Birchall, J. Development of an ex vivo human skin model for intradermal vaccination: Tissue viability and Langerhans cell behaviour. *Vaccine* **2009**, *27*, 5948–5955. [CrossRef]
60. Cappellozza, E.; Zanzoni, S.; Malatesta, M.; Calderan, L. Integrated Microscopy and Metabolomics to Test an Innovative Fluid Dynamic System for Skin Explants In Vitro. *Microsc. Microanal.* **2021**, *27*, 923–934. [CrossRef]
61. Pulsoni, I.; Lubda, M.; Aiello, M.; Fedi, A.; Marzagalli, M.; von Hagen, J.; Scaglione, S. Comparison Between Franz Diffusion Cell and a novel Micro-physiological System for In Vitro Penetration Assay Using Different Skin Models. *SLAS Technol.* **2022**, *27*, 161–171. [CrossRef] [PubMed]
62. Erban, A.; Schauer, N.; Fernie, A.R.; Kopka, J. Nonsupervised construction and application of mass spectral and retention time index libraries from time-of-flight gas chromatography-mass spectrometry metabolite profiles. *Methods Mol. Biol.* **2007**, *358*, 19–38. [PubMed]
63. Roessner, U.; Luedemann, A.; Brust, D.; Fiehn, O.; Linke, T.; Willmitzer, L.; Fernie, A.R. Metabolic Profiling Allows Comprehensive Phenotyping of Genetically or Environmentally Modified Plant Systems. *Plant Cell* **2001**, *13*, 11–29. [CrossRef]
64. Lisec, J.; Schauer, N.; Kopka, J.; Willmitzer, L.; Fernie, A.R. Gas chromatography mass spectrometry–based metabolite profiling in plants. *Nat. Protoc.* **2006**, *1*, 387–396. [CrossRef]
65. Luedemann, A.; Strassburg, K.; Erban, A.; Kopka, J. TagFinder for the quantitative analysis of gas chromatography—Mass spectrometry (GC-MS)-based metabolite profiling experiments. *Bioinformatics* **2008**, *24*, 732–737. [CrossRef] [PubMed]
66. Pundir, C.S.; Malik, M.; Chaudhary, R. Quantification of pyruvate with special emphasis on biosensors: A review. *Microchem. J.* **2019**, *146*, 1102–1112. [CrossRef]
67. Solano, F. Metabolism and Functions of Amino Acids in the Skin. *Adv. Exp. Med. Biol.* **2020**, *1265*, 187–199.
68. Ivanova, I.E. UVA-Induced Metabolic Changes in Non-Malignant Skin Cells and Ex Vivo Cultured Murine Skin. Ph.D. Thesis, University of Regensburg, Regensburg, Germany, 2024.
69. Llibre, A.; Kucuk, S.; Gope, A.; Certo, M.; Mauro, C. Lactate: A key regulator of the immune response. *Immunity* **2025**, *58*, 535–554. [CrossRef] [PubMed]
70. Barding, G.A., Jr.; Béni, S.; Fukao, T.; Bailey-Serres, J.; Larive, C.K. Comparison of GC-MS and NMR for metabolite profiling of rice subjected to submergence stress. *J. Proteome Res.* **2013**, *12*, 898–909. [CrossRef] [PubMed]
71. Emwas, A.H. The strengths and weaknesses of NMR spectroscopy and mass spectrometry with particular focus on metabolomics research. *Methods Mol. Biol.* **2015**, *1277*, 161–193.
72. Letertre, M.P.M.; Giraudeau, P.; de Tullio, P. Nuclear Magnetic Resonance Spectroscopy in Clinical Metabolomics and Personalized Medicine: Current Challenges and Perspectives. *Front. Mol. Biosci.* **2021**, *8*, 698337. [CrossRef]
73. Liu, D.; Fernandez, B.O.; Hamilton, A.; Lang, N.N.; Gallagher, J.M.; Newby, D.E.; Feelisch, M.; Weller, R.B. UVA irradiation of human skin vasodilates arterial vasculature and lowers blood pressure independently of nitric oxide synthase. *J. Investig. Dermatol.* **2014**, *134*, 1839–1846. [CrossRef]
74. Gralka, E.; Luchinat, C.; Tenori, L.; Ernst, B.; Thurnheer, M.; Schultes, B. Metabolomic fingerprint of severe obesity is dynamically affected by bariatric surgery in a procedure-dependent manner12. *Am. J. Clin. Nutr.* **2015**, *102*, 1313–1322. [CrossRef]

75. Leija, R.G.; Curl, C.C.; Arevalo, J.A.; Osmond, A.D.; Duong, J.J.; Huie, M.J.; Masharani, U.; Brooks, G.A. Enteric and systemic postprandial lactate shuttle phases and dietary carbohydrate carbon flow in humans. *Nat. Metab.* **2024**, *6*, 670–677. [CrossRef] [PubMed]
76. Parkinson, E.K.; Adamski, J.; Zahn, G.; Gaumann, A.; Flores-Borja, F.; Ziegler, C.; Mycielska, M.E. Extracellular citrate and metabolic adaptations of cancer cells. *Cancer Metastasis Rev.* **2021**, *40*, 1073–1091. [CrossRef] [PubMed]
77. Hornig-Do, H.-T.; von Kleist-Retzow, J.-C.; Lanz, K.; Wickenhauser, C.; Kudin, A.P.; Kunz, W.S.; Wiesner, R.J.; Schauen, M. Human Epidermal Keratinocytes Accumulate Superoxide Due to Low Activity of Mn-SOD, Leading to Mitochondrial Functional Impairment. *J. Investig. Dermatol.* **2007**, *127*, 1084–1093. [CrossRef]
78. Gopalan, C.; Kirk, E. Chapter 9—Cellular metabolism. In *Biology of Cardiovascular and Metabolic Diseases*; Gopalan, C., Kirk, E., Eds.; Academic Press: Cambridge, MA, USA, 2022; pp. 157–179.
79. He, H.; Xiong, L.; Jian, L.; Li, L.; Wu, Y.; Qiao, S. Role of mitochondria on UV-induced skin damage and molecular mechanisms of active chemical compounds targeting mitochondria. *J. Photochem. Photobiol. B Biol.* **2022**, *232*, 112464. [CrossRef]
80. Ming, D.; Jangam, S.; Gowers, S.A.; Wilson, R.; Freeman, D.M.; Boutelle, M.G.; Cass, A.E.G.; O'Hare, D.; Holmes, A.H. Real-time Continuous Measurement of Lactate through a Minimally-invasive Microneedle Biosensor: A Phase I Clinical Study. *medRxiv* **2021**. [CrossRef]
81. Wang, X.; Perez, E.; Liu, R.; Yan, L.-J.; Mallet, R.T.; Yang, S.-H. Pyruvate protects mitochondria from oxidative stress in human neuroblastoma SK-N-SH cells. *Brain Res.* **2007**, *1132*, 1–9. [CrossRef]
82. Izumi, Y.; Katsuki, H.; Zorumski, C.F. Monocarboxylates (pyruvate and lactate) as alternative energy substrates for the induction of long-term potentiation in rat hippocampal slices. *Neurosci. Lett.* **1997**, *232*, 17–20. [CrossRef]
83. Park, A.; Kim, W.K.; Bae, K.H. Distinction of white, beige and brown adipocytes derived from mesenchymal stem cells. *World J. Stem Cells* **2014**, *6*, 33–42. [CrossRef]
84. van Diepen, J.A.; Robben, J.H.; Hooiveld, G.J.; Carmone, C.; Alsady, M.; Boutens, L.; Bekkenkamp-Grovenstein, M.; Hijmans, A.; Engelke, U.F.H.; Wevers, R.A.; et al. SUCNR1-mediated chemotaxis of macrophages aggravates obesity-induced inflammation and diabetes. *Diabetologia* **2017**, *60*, 1304–1313. [CrossRef] [PubMed]
85. Genever, P.G.; Maxfield, S.J.; Skerry, T.M.; Kennovin, G.D.; Maltman, J.; Bowgen, C.J.; Raxworthy, M.J. Evidence for a novel glutamate-mediated signaling pathway in keratinocytes. *J. Investig. Dermatol.* **1999**, *112*, 337–342. [CrossRef]
86. Fischer, M.; Glanz, D.; Urbatzka, M.; Brzoska, T.; Abels, C. Keratinocytes: A source of the transmitter l-glutamate in the epidermis. *Exp. Dermatol.* **2009**, *18*, 1064–1066. [CrossRef]
87. Liss, D.B.; Paden, M.S.; Schwarz, E.S.; Mullins, M.E. What is the clinical significance of 5-oxoproline (pyroglutamic acid) in high anion gap metabolic acidosis following paracetamol (acetaminophen) exposure? *Clin. Toxicol.* **2013**, *51*, 817–827. [CrossRef]
88. Gamarra, Y.; Santiago, F.C.; Molina-López, J.; Castaño, J.; Herrera-Quintana, L.; Domínguez, Á.; Planells, E. Pyroglutamic acidosis by glutathione regeneration blockage in critical patients with septic shock. *Crit. Care* **2019**, *23*, 162. [CrossRef]
89. Zou, Y.; Cao, M.; Tao, L.; Wu, S.; Zhou, H.; Zhang, Y.; Chen, Y.; Ge, Y.; Ju, Z.; Luo, S. Lactate triggers KAT8-mediated LTBP1 lactylation at lysine 752 to promote skin rejuvenation by inducing collagen synthesis in fibroblasts. *Int. J. Biol. Macromol.* **2024**, *277*, 134482. [CrossRef] [PubMed]
90. Christner, P.; Carpousis, A.; Harsch, M.; Rosenbloom, J. Inhibition of the assembly and secretion of procollagen by incorporation of a threonine analogue, hydroxynorvaline. *J. Biol. Chem.* **1975**, *250*, 7623–7630. [CrossRef] [PubMed]
91. Slominski, A.; Tobin, D.J.; Shibahara, S.; Wortsman, J. Melanin Pigmentation in Mammalian Skin and Its Hormonal Regulation. *Physiol. Rev.* **2004**, *84*, 1155–1228. [CrossRef] [PubMed]
92. Slominski, A.; Zmijewski, M.A.; Pawelek, J. L-tyrosine and L-dihydroxyphenylalanine as hormone-like regulators of melanocyte functions. *Pigment. Cell Melanoma Res.* **2012**, *25*, 14–27. [CrossRef]
93. Smit, N.P.M.; van der Meulen, H.; Koerten, H.K.; Kolb, R.M.; Mommaas, A.M.; Lentjes, E.G.; Pavel, S. Melanogenesis in Cultured Melanocytes can be Substantially Influenced by L-Tyrosine and L-Cysteine. *J. Investig. Dermatol.* **1997**, *109*, 796–800. [CrossRef] [PubMed]
94. Kaur, G.; Dufour, J.M. Cell lines: Valuable tools or useless artifacts. *Spermatogenesis* **2012**, *2*, 1–5. [CrossRef] [PubMed]
95. Aitken, G.R.; Henderson, J.R.; Chang, S.-C.; McNeil, C.J.; Birch-Machin, M.A. Direct monitoring of UV-induced free radical generation in HaCaT keratinocytes. *Clin. Exp. Dermatol.* **2007**, *32*, 722–727. [CrossRef]
96. Li, Q.; Bai, D.; Qin, L.; Shao, M.; Zhang, S.; Yan, C.; Yu, G.; Hao, J. Protective effect of d-tetramannuronic acid tetrasodium salt on UVA-induced photo-aging in HaCaT cells. *Biomed. Pharmacother.* **2020**, *126*, 110094. [CrossRef] [PubMed]
97. Tochio, T.; Tanaka, H.; Nakata, S. Glucose transporter member 1 is involved in UVB-induced epidermal hyperplasia by enhancing proliferation in epidermal keratinocytes. *Int. J. Dermatol.* **2013**, *52*, 300–308. [CrossRef]
98. Manosalva, C.; Bahamonde, C.; Soto, F.; Leal, V.; Ojeda, C.; Cortés, C.; Alarcón, P.; Burgos, R.A. Linoleic Acid Induces Metabolic Reprogramming and Inhibits Oxidative and Inflammatory Effects in Keratinocytes Exposed to UVB Radiation. *Int. J. Mol. Sci.* **2024**, *25*, 10385. [CrossRef]

99. Weihs, P.; Schmalwieser, A.; Reinisch, C.; Meraner, E.; Walisch, S.; Harald, M. Measurements of personal UV exposure on different parts of the body during various activities. *Photochem. Photobiol.* **2013**, *89*, 1004–1007. [CrossRef] [PubMed]
100. Mildner, M.; Jin, J.; Eckhart, L.; Kezic, S.; Gruber, F.; Barresi, C.; Stremnitzer, C.; Buchberger, M.; Mlitz, V.; Ballaun, C.; et al. Knockdown of filaggrin impairs diffusion barrier function and increases UV sensitivity in a human skin model. *J. Investig. Dermatol.* **2010**, *130*, 2286–2294. [CrossRef] [PubMed]